Nanostructured dimethacrylate-based photopolymerizable systems by modification with diblock copolymers

Article

Accepted Version

Malafronte, A. ORCID: https://orcid.org/0000-0002-7854-5823, Hamley, I. W. ORCID: https://orcid.org/0000-0002-4549-0926, Hermida-Merino, D. ORCID: https://orcid.org/0000-0002-8181-158X, Auriemma, F. and De Rosa, C. ORCID: https://orcid.org/0000-0002-5375-7475 (2021) Nanostructured dimethacrylate-based photopolymerizable systems by modification with diblock copolymers. Polymer, 237. 124360. ISSN 0032-3861 doi: 10.1016/j.polymer.2021.124360 Available at https://centaur.reading.ac.uk/101445/

It is advisable to refer to the publisher's version if you intend to cite from the work. See Guidance on citing.

Nanostructured Dimethacrylate-based Photopolymerizable Systems by Modification with Diblock Copolymers

Anna Malafronte, Ian W. Hamley, Daniel Hermida-Merino, Finizia Auriemma, and Claudio De Rosa

Dr. A. Malafronte, Prof. F. Auriemma, Prof. C. De Rosa
Dipartimento di Scienze Chimiche, Università degli Studi di Napoli Federico II, Complesso Monte S. Angelo, Via Cintia, 80126, Napoli, Italy
E-mail: ((insert e-mail address(es) of corresponding author(s)))

Prof. I. W. Hamley
Department of Chemistry, University of Reading, Reading, RG6 6AD, United Kingdom

Dr. D. Hermida-Merino
European Synchrotron Radiation Facility (ESRF), 6 rue Jules Horowitz, BP 220, 38043 Grenoble Cedex 9, France

We report the full characterization of a photocurable dimethacrylate-based formulation modified with small amounts (1 – 6 wt%) of a polystyrene-*block*-poly(ethylene oxide) (PS-*b*-PEO) block copolymer (BCP). The UV curable formulation is a mixture of bisphenol A bis(2-hydroxy-3-methacryloxypropyl)ether (Bis-GMA) and triethylene glycol dimethacrylate (TEGDMA) and contains phenylbis(2,4,6-trimethylbenzoyl)phosphine oxide (Irgacure819) as photoinitiator. We demonstrate that the addition of a small amount of BCP in the uncured formulation is able to induce a phase separation at the nanometer scale. The nanoscale structure formed in the pre-cure stage is retained after the UV curing, so obtaining nanostructured solid cross-linked materials. The studied materials can be used in the manufacturing process of stereolithography and, therefore, in modern 3D printers. The ability to induce and control the formation of nanostructures in the material by adding BCPs in the formulations could open new opportunities to tailor and improve the properties of the 3D printed objects.

1. Introduction

The polymerization of liquid monomers or oligomers (precursors) to produce solid densely cross-linked networks (resin), finds a wide range of applications in curing processes in different fields[1-6] such as the fabrication of structural adhesives, surface coatings, elastomeric impression materials,[2] as well as in dentistry (dental composites, dentine bonding agents, pit and fissure sealants, cements)[3-5] and in emerging additive manufacturing (*i.e.* 3D printing).[6] Chemical reactions initiating the curing process can be triggered by heat (thermal curing), pressure, change in pH, or radiation (electron beam exposure, gamma-radiation and light). The radiation curing process (photopolymerization) shows different advantages compared to the other curing methods, such as the speed at which the final product can be obtained, lower process costs, high chemical stability and solvent-free curing at ambient temperatures. Currently, photocurable dimethacrylate-based formulations represent the large majority of all commercial resins used in dental composite restorative materials[3-5] and dominate research into materials to be employed in 3D printing photopolymerization-based processes (such as stereolithography and digital light processing).[6] The dominant chemistry for light curing is the radical polymerization of unsaturated precursors containing unsaturated acrylates, and the predominant base monomer used in many commercial materials is bisphenol A bis(2-hydroxy-3-methacryloxypropyl)ether (Bis-GMA) **(Figure 1A)**, which due to its high viscosity is mixed with other dimethacrylates, such as triethylene glycol dimethacrylate (TEGDMA) **(Figure 1B)**.[7-9] An appropriate photoinitiator, able to absorb light (in the ultraviolet, UV, or visible range) and undergo a photoreaction that produces the reactive energetic radical species capable of initiating the polymerization of the unsaturated functionalities of the monomers, is added to the light-curable formulation. It is worth noting that the term "resin" is often applied to both the precursors (containing reactive groups) and to the cured materials (cross-linked networks).[2] The most used photoinitiator system in visible light-activated composite resins is

camphorquinone (CQ), coupled with reducing agents represented by tertiary amines.[10] Some commercial UV-curable formulations include other photoinitiators, such as phenylbis(2,4,6-trimethylbenzoyl)phosphine oxide (Irgacure819) (**Figure 1C**).[11]
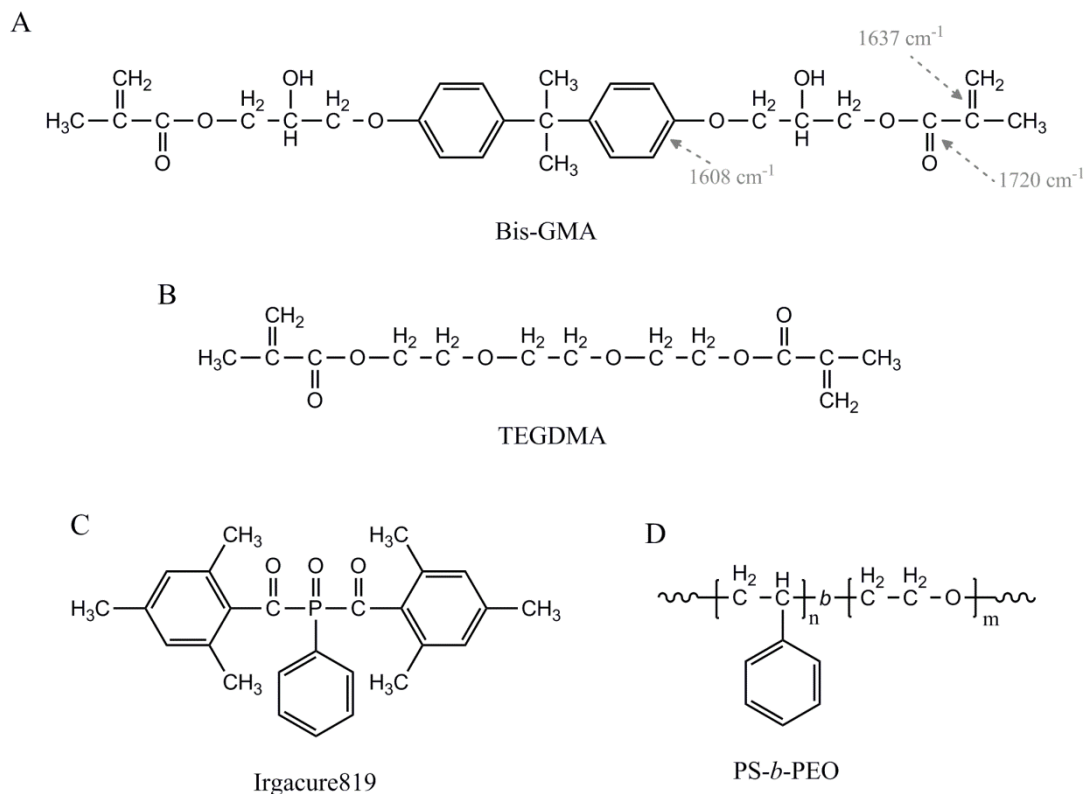
A

Bis-GMA

B

TEGDMA

C

Irgacure819

D

PS-*b*-PEO

Figure 1. Chemical structures of the materials used in the present work; (A) Bisphenol A, bis(2-hydroxy-3-methacryloxypropyl)ether (Bis-GMA); (B) Triethyleneglycol dimethacrylate (TEGDMA); (C) The photoinitiator phenylbis(2,4,6-trimethylbenzoyl)phosphine oxide (Irgacure819) and (D) polystyrene-*block*-poly(ethylene oxide) copolymer (PS-*b*-PEO). In (A) the absorption infra-red (IR) wavenumbers of some relevant groups are indicated: 1608 cm^{-1} (aromatic C=C bonds), 1637 cm^{-1} (C=C stretching) and 1720 cm^{-1} (carbonyl stretching vibration).

In order to achieve the desired properties in the final resins, including enhanced modulus, radiopacity, controlled thermal expansion behavior and reduced polymerization shrinkage, filler contents of 60 to 87 wt% are necessary.[3, 12, 13] Inorganic nanocomponents (silica, glass,

alumina, zirconia and titania nanoparticles), a variety of sol-gel-derived hybrid organic/inorganic monomers (ormocers) as well as functional silanes have been included in the formulations.[12] The role of each component (the polymerizable resin, the filler, and the filler-resin interface) in dictating the final properties of the material has been extensively explored and the benefits of the incorporation of nanomaterials in the resins has been demonstrated. The final properties of the composite are determined by the properties of the components, by the amount of filler added and the size and form of the particles, by the morphology of the system, and by the nature of the interface between the phases. A great variety of properties can be obtained by changing one of the components.

Despite the high relevance to applications, less attention has been devoted to the study of the incorporation of nanostructured inclusions in UV-curable resins to be used in 3D printing processes[14, 15] such as stereolithography, in which high intensity UV light is used to initiate a photochemical reaction that instantly cures a liquid formulation allowing building, by means of an additive manufacturing process, layer by layer, a complete solid 3-D object.[16] While researchers have experimented with the addition of inorganic microscale particles (sizes ≥ 100 nm),[17,18] published research combining 3D printing and nanomaterials is quite limited.[15] To the best of our knowledge, no example is reported regarding the evaluation of block copolymers (BCPs), able to spontaneously generate nanostructures by self-assembly, as organic additives in photopolymerizable formulations.
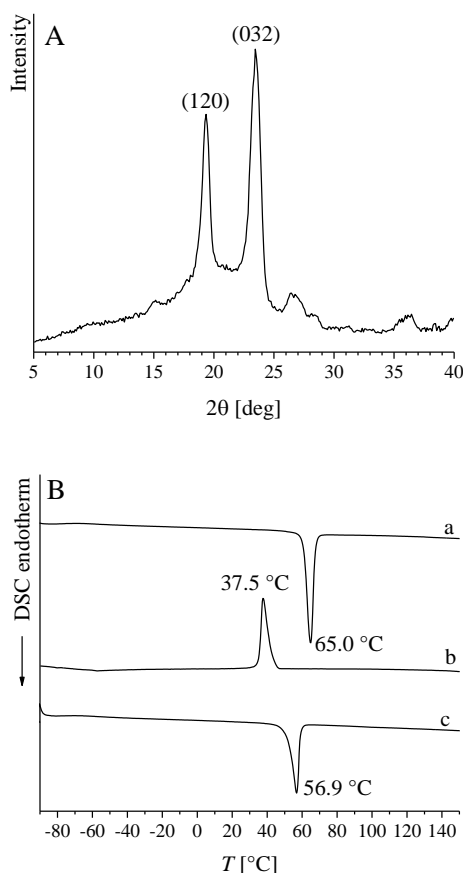
BCPs can self-assemble into a wide variety of nanostructures, with a typical length scale in the range 10-100 nm, in bulk or in solution.[19,21] In bulk, BCPs with immiscible blocks can microphase separate as a function of composition into a variety of morphologies, including spheres, cylinders, lamellae, bicontinuous gyroid and other structures. In solution, a wide range of aggregates of different morphologies can be obtained from amphiphilic BCP systems including spherical micelles, rods, bicontinuous structures, lamellae, vesicles, large compound micelles (LCMs), large compound vesicles (LCVs), tubules, "onions", "eggshells", etc. By

tuning molecular parameters (chemical nature of blocks, molecular mass, composition, concentration) nanometer-scale features with a variety of motifs, chemistries, tailored size and periodicity may be created.[19-21] The BCP-based tailor-made nanostructured materials can be used as nanoscopic device components, as templates for fabrication of nanocomposites,[22-25] or for fabrication of nanoporous thin films with controlled morphology at nanoscale,[26-28] or fabrication of drug delivery systems.[29]

In the present work, we report a full characterization of a UV photopolymerizable formulation modified with small amounts of a polystyrene-*block*-poly(ethylene oxide) (PS-*b*-PEO) block copolymer. We demonstrated that the addition of a small amount of BCP in the uncured formulation is able to induce a phase separation at the nanometer scale. The nanoscale structure formed in the pre-cure stage is retained after the UV curing, so obtaining nanostructured solid cross-linked materials that can be used in the manufacturing process of stereolithography and, therefore, they can be used in modern 3D printers. The formulation consists of a mixture of Bis-GMA (Figure 1A) and TEGDMA (Figure 1B) and contains the molecule Irgacure819 (Figure 1C) as photoinitiator. We used different experimental techniques such as Fourier transform infrared spectroscopy (FT-IR), differential scanning calorimetry (DSC), small-angle X-ray scattering (SAXS) and transmission electron microscopy (TEM) to characterize the neat formulation and the formulation containing the BCP at different concentrations (between 0 and 6 wt%) before and after UV curing. Although some literature examples are reported regarding the study of block copolymers as additives in epoxy resins to fabricate nanostructured thermally cured systems (thermosets),[30,31] to best of our knowledge, this is the first work concerning the study UV of photopolymerizable dimethacrylate systems modified with a di-block copolymer.

2. Results and Discussion

5

The polystyrene-*block*-poly(ethylene oxide) (PS-*b*-PEO) copolymer used as additive of the UV photocurable resins **(Figure 1D)** is semicrystalline, PEO and PS being the semicrystalline and amorphous blocks, respectively, as confirmed by the wide-angle X-ray scattering (WAXS) profile of the sample **(Figure 2A)** showing two main diffraction peaks centered at $2\theta(CuK_\alpha) \approx 19$ and $23°$, respectively, corresponding to the (120) and (032) reflections of the monoclinic form of PEO,[32,33] superposed on an amorphous halo due to the contributions of the amorphous phases of the PEO and PS blocks. The DSC thermograms **(Figure 2B)** indicates that the semicrystalline PEO blocks melt at 65.0 °C (curve a of Figure 2B), crystallize by cooling from the melt at 37.5 °C (curve b of Figure 2B) and, finally, the melt-crystallized sample melts at 56.9 °C (curve c of Figure 2B). The glass transition temperatures (T_g) of PS and PEO blocks, expected to be ≈ 107 and $\approx$ -65 °C, respectively,[34,35] are not well discernible from the acquired DSC data.
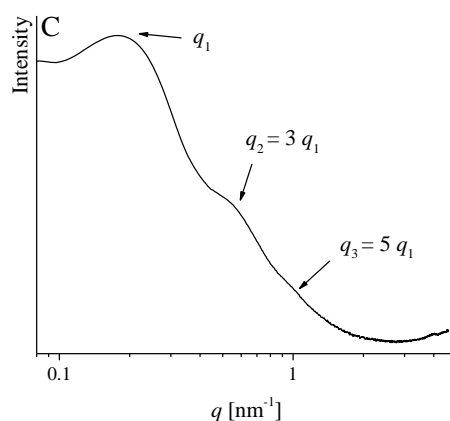
Figure 2. Room temperature WAXS profile (A), DSC curves (B) recorded at scanning rate of 10 °C/min during (a) first heating, (b) cooling from the melt and (c) successive second heating, and (C) room temperature SAXS profile on a logarithmic scale of the as received PS-*b*-PEO BCP. A scanning rate of 10 °C min^{-1} was used to acquire the DSC data. The (120) and (032) reflections of the monoclinic form of PEO and the melting and crystallization temperatures of PEO are indicated in A and B, respectively. In C the peaks at $q_2 = 3q_1$ and $q_3 = 5q_1$ typical of the lamellar morphology are indicated, where q is the modulus of the scattering vector equal to $q = 4\pi \sin \theta / \lambda$.

The room temperature small-angle X-ray scattering (SAXS) profile of the as received PS-*b*-PEO BCP is reported in **Figure 2C**. Multiple orders of Bragg reflection are observed, indicating a nanoscale phase separated morphology. In particular, the first (1), third (3) and fifth (5) order reflections of the lamellar (Lam) morphology appear, as expected for a BCP with volume fraction of blocks around 50%.[19-21] SAXS positions of the peaks and the lamellar periodicity are reported in Table 2 (*vide infra*).

We prepared, according to the procedure described in the Experimental Section, four different formulations (Table 1). The first of them, named "neat resin", contains the two acrylate monomers (Bis-GMA and TEGMA, Figure 1A and B, respectively) and the photoinitiator Irgacure819 (Figure 1C). The other three samples contain the same components and, in

addition, the PS-*b*-PEO BCP (Figure 1D) at different concentrations, that is 1, 3 and 6 wt%. These samples are named "resin-BCP1", "resin-BCP3" and "resin-BCP6", respectively (Table 1). The PEO block of the BCP has a structural analogy, and therefore miscibility, with one component of the resin precursors (TEGDMA) (Figure 1D and B) and that the two dimethacrylate precursors (BisGMA and TEGDMA, Figure 1A and B, respectively) are amorphous (Figure S1) with values of T_g equal to - 7.7 and -83.4 °C, respectively.[7]

Table 1. Compositions, glass transition temperatures before curing (T_g) and degrees of conversions after 6 min UV irradiation (DC_{6min}) of the studied formulations. Bisphenol A bis(2-hydroxy-3-methacryloxypropyl)ether (Bis-GMA) and Triethyleneglycol dimethacrylate (TEGDMA) were always used in a ratio 50 : 50 by weight. The amount of the photoinitiator (Irgacure819) is the same in all the samples.

Sample name	Sample composition [wt%]		T_g [°C]	DC_{6min} [%]
	BisGMA + TEGDMA	PS-*b*-PEO		
Neat resin	100	0	-64.9	47.9 ± 0.8
Resin-BCP1	99	1	-64.7	45 ± 1
Resin-BCP3	97	3	-64.2	47 ± 1
Resin-BCP6	94	6	-63.7	45.2 ± 0.9

Fourier transform infrared (FT-IR) spectroscopy was used to determine the degree of conversion (*DC*) of the samples (Table 1) by using Equation 1 (Experimental Section). FT-IR spectra were recorded for each sample at zero time (before curing) and immediately after a fixed time of exposure to UV-light (curing time). The obtained spectra in the case of the neat resin and of the sample containing 6 wt% BCP (Resin-BCP6) are reported in Figure S2A and B, respectively, as an example. The assignments of main FTIR peaks are reported in Table S1. The most significant signals in our study occur in the range 1800-1550 cm^{-1}. Magnifications of this region in the case of the samples before curing and after curing for 5 *s* are reported in

Figure 3A and **Figure 3B** (curves a and b, respectively). In this region, signals from the aromatic C=C bond (1608 cm^{-1}), the aliphatic C=C stretching (1637 cm^{-1}) and the carbonyl stretching vibration (1720 cm^{-1}) appear (Figure 1A and Table S1). The amount of double vinyl bonds remaining in the sample exposed to irradiation is shown by the intensity of the peak at 1637 cm^{-1} relative to the aromatic C=C stretching peak. The intensity of this peak, in fact, decreases during the photopolymerization (Figure 3). It is worth noting that during the photopolymerization also the position and the intensity of the peak at 1720 cm^{-1} (assigned to the carbonyl stretching vibration) changes (Figure 3). In the uncured state the carbonyl group is conjugated with the C=C bond (see Figure 1A and B) and upon curing this conjugation is lost. This results in a slight shift of the carbonyl peak to higher wavenumbers in the cured state, as the bond becomes stronger, owing to the fact that the electrons are no longer delocalized. A simultaneous decrease of this peak is also observed in the cured state.
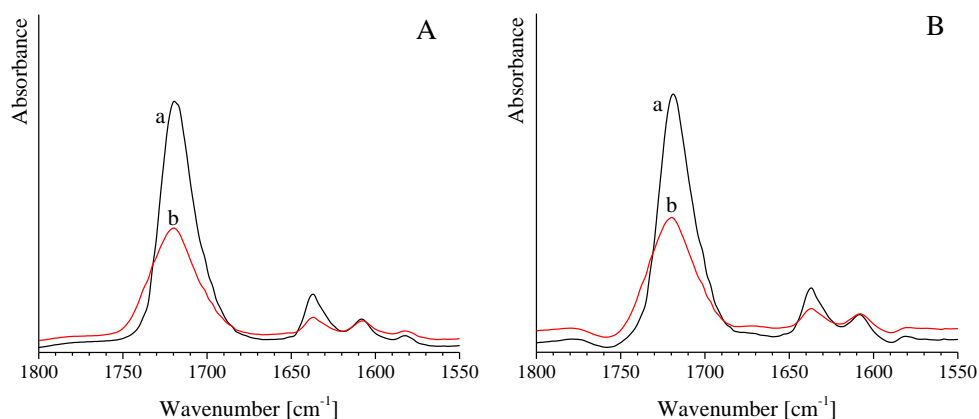

Figure 3. FT-IR spectra in the 1800-1550 cm^{-1} range of the neat resin (A) and of the resin-BCP6 sample (B), before (a) and after (b) UV curing for 5 s.

The degrees of conversion as a function of curing time for all the samples are shown in **Figure 4** and reported in Table S2. The *DC* obtained after an irradiation time equal to 6 min are also reported in Table 1. The lowest explored curing time in the case of the samples containing 1 and 3 wt% BCP was 2 min (curves b and c of Figure 4, respectively). In the case of the neat

resin (curve a of Figure 4) and of the sample containing 6 wt% BCP (resin-BCP6, curve d of

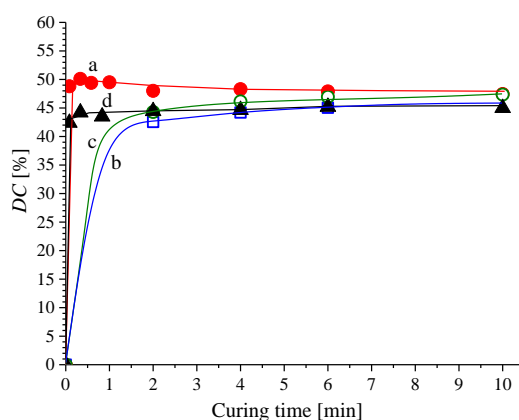Figure 4) curing times lower than 2 min were also explored.

Figure 4. Degrees of conversion (*DC*) *vs* UV curing time for the neat resin (●, a) and samples

containing the BCP: resin-BCP1 (□, b), resin-BCP3 (○, c) and resin-BCP6 (▲, d) containing

1, 3 and 6 wt% BCP, respectively. The lines are guide for eyes. Error bars have been removed

for clarity. The explored curing times for each sample and the corresponding *DC* values are

reported in Table S2. The *DC*s obtained after an irradiation time equal to 6 min are also reported

in Table 1.

The photopolymerization, under the employed experimental conditions, is a quite fast process,

since the degree of conversion reaches already a plateau after short UV irradiation times,

corresponding to 5 s in the case of the neat resin and resin-BCP6 sample containing 6 wt% BCP

(curves a and d of Figure 4). In particular, after 5 s of polymerization, 48.8% and 42.4% of the

double bonds have reacted in the neat resin and the sample containing 6 wt% BCP and, after 2

min of polymerization, a degree of conversion of 43 and 44 % is reached in the case of the

samples containing 1 and 3 wt% BCP, respectively (Table S2). The rate of the

photopolymerization process makes the investigated formulations compatible with the

manufacturing process of stereolithography and, therefore, we successfully tested the materials

in Asiga 3D printer (Figure S3). The introduction of the block copolymer doesn't significantly

influence the degree of conversion of the resin. After 6 min of UV-irradiation time, in fact, the neat resin shows a *DC* equal to 47.9 %, only slightly higher than the *DC* evaluated for the BCP containing samples, equal to 45, 47 and 45.2 % in the case of the samples containing 1, 3 and 6 wt% of BCP, respectively (Table 1 and S2). The obtained *DC* values may be considered good. The room-temperature polymerization of dimethacrylates, in fact, usually leads to glassy resins in which only a part of the available double bonds are reacted. This is due to the fact that the mobility of the reacting medium decreases as the polymerization proceeds. In particular, as the degree of cross-linking increases, the propagation step, which involves the reaction of small monomer molecules with macroradicals, becomes more difficult because unreacted pendant double bonds, macroradicals and free monomer become trapped among network units and completely immobilized. As a consequence, these systems are characterized by a maximum limiting conversion significantly less than unity.[7]

The differential scanning calorimetry (DSC) characterization of the samples is reported in **Figure 5**. In particular, the first heating and cooling DSC curves of the four mixtures (Table 1) before curing are reported in Figure 5A and A', respectively. The DSC thermograms show no significant peak for any reaction or transition with increasing temperature. This confirms that the resins cannot be thermally cured, at least over this temperature range. All the samples display a glass transition temperature (T_g) equal to $\approx$ - 65.0 °C, typical of a 50/50 (wt%) TEGDMA/Bis-GMA uncured mixture.[7] As previously discussed, PEO is a semicrystalline polymer with a melting temperature of 65.0 °C (curve a of Figure 2B). The absence of melting and crystallization peaks in the DSC thermograms of samples containing the BCP (curves b-d of Figure 5A and A') suggests that the PEO block is unable to crystallize because PEO chains are well dispersed in the acrylate formulations.
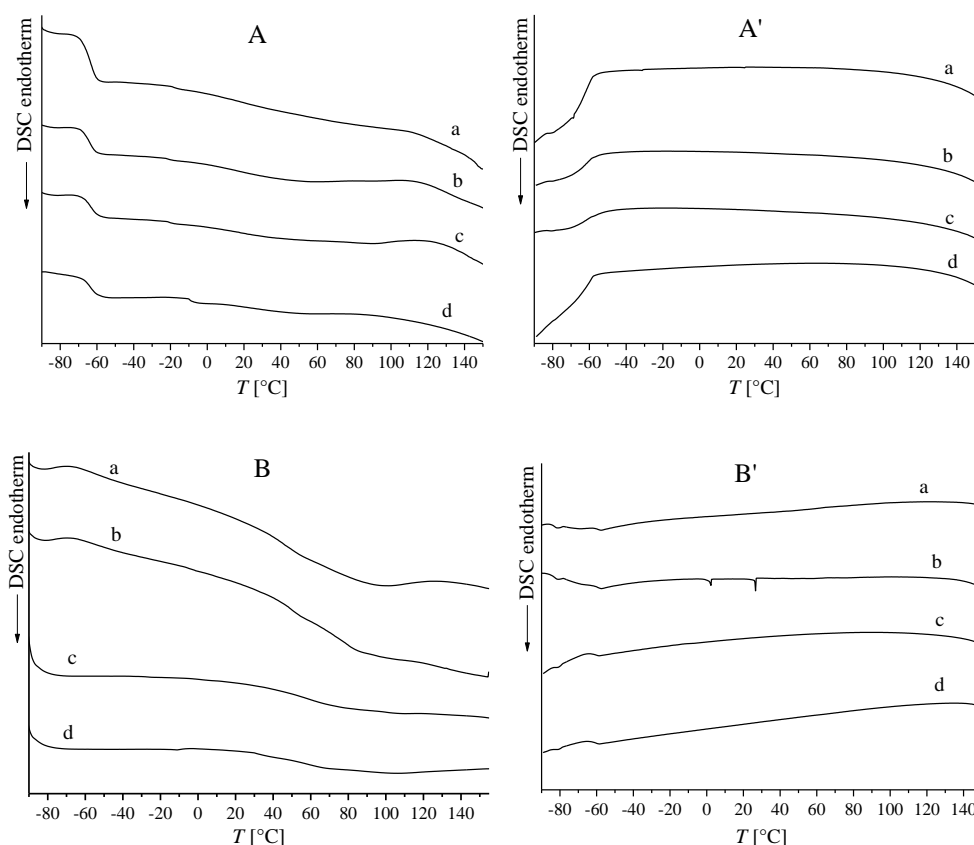
Figure 5. First heating (A, B) and cooling (A', B') DSC scans of the samples before (A, A') and after (B, B') curing; neat resin (curves a), resin-BCP1 (curves b), resin-BCP3 (curves c) and resin-BCP6 (curves d). Scanning rate, 10 °C/min.

The first heating and cooling DSC curves of the four mixtures (Table 1) after UV curing for ≈ 5 min are reported in Figure 5B and B', respectively. As expected, the DSC thermograms dramatically change after the curing of the samples. All specimens show a broad endotherm, centred at around 80 °C, in the first heating scans (Figure 5B) that can be due either to the occurrence of further cross-linking reactions activated by the increase of mobility during heating and/or to the large heterogeneities segmental dynamics at the glass transition temperature (T_g) of the partially cross-linked networks.[36] No relevant transition is detected in the cooling scans (Figure 5B'), confirming that the heating of the UV cured samples increases the cross-linking density of the network.

The room temperature SAXS profiles of the neat resin and of the samples containing 1 and 3 wt% BCP acquired before curing are reported in **Figure 6A**. No peaks appear in the SAXS profile of the neat resin (curve a of Figure 6 A), indicating the absence of phase separation at the nanoscale due to complete miscibility between the components of the resin (BisGMA and TEGDMA). Scattering peaks are instead observed for the samples containing the BCP, indicating the presence of a phase separation at the nanometer length scale. In particular, one broad peak centered at 0.23 nm^{-1} is observed in the case of the sample containing 1 wt% BCP (curve b of Figure 6A) whereas two peaks centered at 0.14 and 0.24 nm^{-1} are present in the SAXS profile of the sample containing 3 wt% BCP (curve c of Figure 6A). The SAXS positions of the peaks and the domain spacing corresponding to the peaks (d_i) are reported in Table 2.
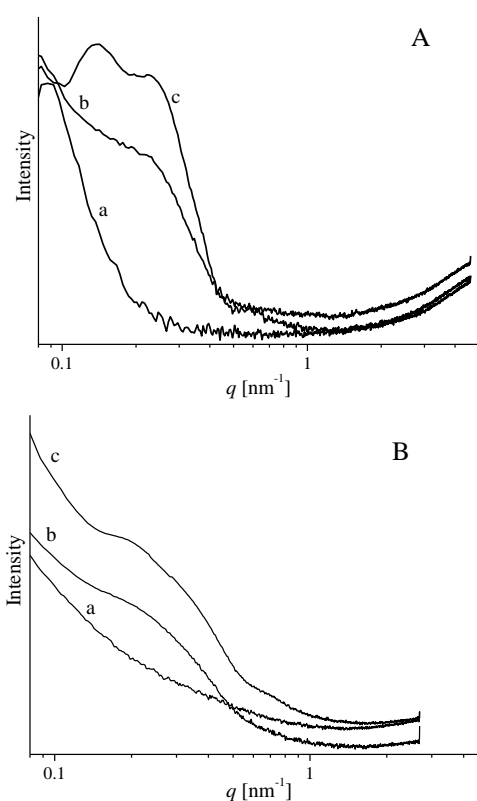

Figure 6. Room temperature SAXS profiles in logarithmic scale before (A) and after (B) curing of the neat resin (curves a), the resin-BCP1 (b) and the resin-BCP3 (c) samples.

Since the mixtures of photopolymerizable resin precursors and PS-*b*-PEO BCP are transparent at room temperature, no phase separation occurs at the macroscopic scale. However, at the nanoscale, the good miscibility of PEO with Bis-GMA and TEGDMA and the low compatibility of PS with the mixture probably leads to formation of micellar aggregates characterized by a PS core with PEO chains at the interface with the uncured photopolymerizable components.

Table 2. SAXS peak positions ($q=4\pi \sin \theta/\lambda$) and *d*-spacings (*d*) for the indicated samples. Values obtained from the SAXS profiles of Figure 2C and Figure 6.

Sample	q_1 [nm^{-1}]	q_2 [nm^{-1}]	q_3 [nm^{-1}]	d_1, d_2, d_3 [nm]
Neat BCP[a]	0.19	0.56	0.95	33, 11, 7
Resin-BCP1 before curing	0.23	-	-	27
Resin-BCP3 before curing	0.14	0.24	-	45, 26
Resin-BCP1 after curing	0.27	-	-	23
Resin-BCP3 after curing	0.21	0.37[b]	-	30

[a] $q_2 = 3\ q_1$ and $q_3 = 5\ q_1$; [b] Shoulder

The SAXS profiles acquired after UV curing are reported in **Figure 6B**. Again, no scattering peaks are observed in the case of the neat resin (curve a of Figure 6B) indicating that the cured system in absence of BCP remains isotropic at the nanometer length scale. Broad peaks appear in the profiles of the samples containing the BCP (curves b and c of Figure 6B) suggesting that the nanoscale structure formed in the pre-cure stage (Figure 6A) is retained after the UV curing. In particular, a broad peak, corresponding to a spacing of 23 nm, is present in the sample containing 1 wt% BCP (curve b of Figure 6B) as in the case of the profile acquired before curing (curve b of Figure 6A). In the case of the sample containing 3 wt% BCP (curve c of Figure 6B), a broad peak at 0.21 nm^{-1} and a faint shoulder at ≈ 0.37 nm^{-1} appear. Therefore, the morphology of the corresponding uncured mixture (curve c of Figure 6A) is only partly retained in the cured

system probably because the cross-linking reaction induces a partial break-out of the initial nanostructure.

The presence of phase separation at nanometer scale in the case of the sample containing the BCP has been confirmed by transmission electron microscopy (TEM). A representative TEM image of a thin section of sample containing 3 wt% BCP after 10 min UV curing is reported in **Figure 7**.
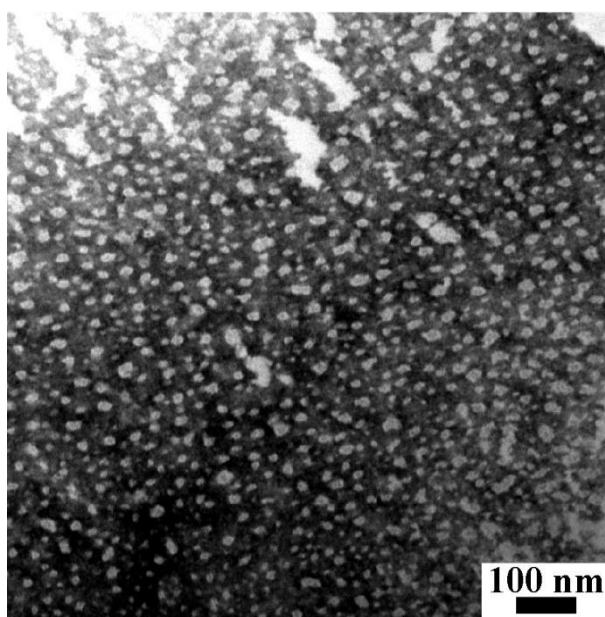

Figure 7. TEM image of 70 thin section of the sample containing 3 wt% BCP after 10 min UV curing. Staining with uranyl acetate was performed before the TEM observation.

The presence of a nano phase separation is evident (Figure 7). Bright pseudo-spherical domains with diameters ranging from 10 to 25 nm, most likely due to PS aggregates, appear in a dark matrix. The center-to-center distance between the bright domains obtained from TEM image of Figure 7 ($\approx$ 30 nm) well agrees with the dimensions obtained from the SAXS data (Table 2), confirming the hypothesis that PS domains tend to form micellar aggregates fringed with PEO chains. No phase separation was instead observed in the case of the neat resin (data not shown).

3. Conclusion

An investigation of acrylate photopolymerizable formulations modified with small amounts of PS-*b*-PEO block copolymer was conducted. Nanostructured systems were obtained by adding the BCP in the formulations, without strong alteration in the capability of the resin to photopolymerize. The nanoscale organization is present both before and after the UV-induced photopolymerization and is due to the good miscibility of PEO blocks with the components of the photopolymerizable formulations (Bis-GMA and TEGDMA) and the low compatibility of PS with the other components. The formation of micellar aggregates characterized by a PS core covalently linked to PEO chains placed at the interface with the photopolymerizable components was confirmed by TEM imaging. Our experimental findings are interesting for the study of processing-morphology-property relationships in these complex systems and to develop methods for creating structures of controlled length scales that would result in materials with tailored and improved properties for 3D printing applications. By leveraging the tunable properties of nanostructures, the material properties and, as consequence, applications of printed components, can be expanded. In addition, the introduction of BCPs able to coordinate nanofillers (such as metal nanoparticles), for example, can avoid the aggregation of the nanofillers in printing media and can lead to the formation of core-shell nanostructures where the core contains the nanofiller and the shell consists of the printing material. These nanostructures could improve the density of the final parts and provide printing materials that possess additional properties, such as electrical and thermal conductivities, since the characteristics of the nanofillers embedded into the printing material are preserved.

4. Experimental Section

Materials: Bisphenol A bis(2-hydroxy-3-methacryloxypropyl)ether (Bis-GMA), Triethyleneglycol dimethacrylate (TEGDMA) and photoinitiator Phenylbis(2,4,6-trimethylbenzoyl)phosphine oxide (Irgacure819) were purchased from Sigma-Aldrich. The symmetric block copolymer polystyrene-*block*-poly(ethylene oxide) (PS-*b*-PEO) with number

average molecular mass (M_n in Kg mol^{-1}) of 22.0-*b*-21.5, polydispersity of 1.09 and volume fraction of blocks ≈ 50 %, was purchased from Polymer Source Inc. All the materials were used as received without further purification.

Preparation of the samples: Four mixtures of the materials (Figure 1) were prepared, the composition of which is shown in Table 1. Bis-GMA and TEGDMA were always used in a ratio 50:50 by weight. They were vigorously stirred for a few minutes at around 60 °C and then at room temperature until the mixture appeared clear. The block copolymer PS-*b*-PEO was added in the mixture BisGMA/TEGDMA, and the resulting mixture was vigorously stirred at 65 °C for at least 7 hours. Using this procedure, samples without block copolymer (neat resin) and samples containing 1, 3 and 6 wt% of BCP (resin-BCP1, resin-BCP3 and resin-BCP6) were prepared (Table 1). Then, to make the samples UV-light curable, a fixed amount of the photoinitiator Irgacure819 (0.5 wt% with respect to the photocurable resin precursors, that is the total Bis-GMA and TEGDMA) was added to each sample. Also in this case, magnetic stirring was used until homogenous, clear yellow systems were obtained. Photopolymerization was performed by irradiating the samples by a UV light source with a maximum emission wavelength at 365 nm, corresponding to the absorption maximum of the Irgacure819 photoinitiator.[11, 37]

Fourier transform infrared spectroscopy (FT-IR) measurements: FT-IR measurements were performed by using a Thermo Scientific Nicolet iS5 FT-IR Spectrometer. A small drop of each sample was placed between two translucent polyethylene strips, which were pressed between two CaF$_2$ crystals to produce a very thin layer. Polyethylene film was used mainly to avoid adhesion of the cured resin on CaF$_2$ crystals and also to prevent oxygen inhibition of polymerization. The samples were irradiated for successive periods of time. The FT-IR spectra were recorded at zero time (before curing) and immediately after each period of exposure to UV-light, in transmission with 128 scans at a resolution of 4 cm^{-1}. The degree of conversion

(*DC*), directly related to the decrease of the absorption band at 1637 cm^{-1} (assigned to the aliphatic C=C stretching), was calculated, as a function of curing time, using Equation 1:

$$DC(\%) = \left(1 - \frac{R_{cured}}{R_{uncured}}\right)x100 \quad \text{where} \quad R = \frac{A_{1637cm^{-1}}}{A_{1608cm^{-1}}} \quad (1)$$

where $A_{1637\,cm^{-1}}$ is the absorption value at 1637 cm^{-1} and $A_{1608\,cm^{-1}}$ is the absorption at 1608 cm^{-1} (assigned to aromatic C=C bonds). The peak at 1608 cm^{-1} was used as internal standard as this adsorption band does not change as a consequence of polymerization.[7,10] The data were averaged over at least three independent measurements experiments.

Differential scanning calorimetry (DSC) experiments: DSC analysis was carried out by using a TA Instruments DSC Q2000 apparatus in a flowing N$_2$ atmosphere. A scanning rate of 10 °C min^{-1} was used to acquire the first heating and cooling scans of the as received BCP and of the four samples reported in Table 1 both before and after UV curing for ≈ 5 min.

Wide- and Small-Angle X-ray Scattering (WAXS and SAXS) measurements: WAXS data were collected using an Empyrean diffractometer (PANalytical) in the reflection geometry, with Ni-filtered CuK$_\alpha$ radiation (wavelength λ =0.15418 nm). SAXS measurements were performed at room temperature on beam line BM26B (DUBBLE) located at the European Synchrotron Radiation Facility (ESRF) in Grenoble, France. A sample-detector distance of 2 m and a wavelength of 1.033 Å were employed to acquire the data. The sample holder scattering was subtracted from each measurement.

Transmission electron microscopy (TEM) imaging: TEM analysis was carried out in bright-field mode using a Philips EM 208S TEM with an accelerating voltage of 100 kV. Ultrathin (70 nm thick) sections of the cured samples were obtained at room temperature using a Reichert-Jung Ultracut E Ultramicrotome equipped with a diamond knife. The thin sections were picked up on carbon-coated Cu grids and stained with uranyl acetate before microscopy observation.

Supporting Information

Supporting Information is available from the Wiley Online Library or from the author.

Acknowledgements

References

[1] L. A. Linden, Radiation curing in polymer science and technology, J. P. Fouassier and J. E. Rabek eds., vol. IV, Essex: Elsevier Ltd 1993.

[2] B. Ellis, Chemistry and technology of epoxy resins, Blackie Academic & Professional, Dordrecht, Springer Netherlands 1993.

[3] N. B. Cramer, J. W. Stansbury, C. N. Bowman, J. *Dent. Res.* **2011**, *90*, 402.

[4] J. L. Ferracane, *Dent Mater.* **2011**, *27*, 29.

[5] N. Moszner, U. Salz, *Macromol. Mater. Eng.* **2007**, *292*, 245.

[6] A. Bagheri, J. Jin, *ACS Appl. Polym. Mater.* **2019**, *1*, 593.

[7] I. Sideridou, V. Tserki, G. Papanastasiou, *Biomaterials* **2002**, *23*, 1819.

[8] P. Ekworapoj, R. Magaraphan, D. C. Martin, *J. Met. Mater. Miner.* **2002**, *12*, 39.

[9] K. L. Van Landuyt, J. Snauwaert, J. De Munck, M. Peumans, Y. Yoshida, A. Poitevin, E. Coutinho, K. Suzuki, P. Lambrechts, B. Van Meerbeek, *Biomaterials* **2007**, *28*, 3757.

[10] H. Arikawa, H. Takahashi, T. Kanie, S. Ban, *Dent. Mater. J.* **2009**, 28, 454.

[11] M. G. Neumann, W. G. Miranda Jr, C. C. Schmitt, F. A. Rueggeberg, I. C. Correa, *J. Dent.* **2005**, *33*, 525.

[12] S. Klapdohr, N. Moszner, *Monatsh. Chem.* **2005**, 136, 21.

[13] U. Lohbauer, R. Frankenberger, N. Kramer, A. Petschelt, J. Biomed. Mater. Res. Part B **2006**, *76*, 114.

[14] T. A. Campbell, O. S. Ivanova, Nano Today **2013**, *8*, 119.

[15] O. Ivanova, C. Williams, T. Campbell, *Rapid Prototyp. J.* **2013**, *19*, 353.

[16] C. W. Hull, *U.S. Patent 4575330*, **1986**.

[17] M. C. George, A. Mohraz, M. Piech, N. S. Bell, J. A. Lewis, P. V. Braun, *Adv. Mater.* **2009**, *21*, 66.

[18] S. S. Nadkarni, J. E. Smay, *J. Am. Ceram. Soc*. **2006**, *89*, 96.

[19] Y. Mai, A. Eisenberg, *Chem. Soc. Rev.* **2012**, *41*, 5969.

[20] F. S. Bates, G. H. Fredrickson, *Annu. Rev. Phys. Chem.* **1990**, *41*, 525.

[21] I. W. Hamley, The Physics of Block Copolymers, Oxford University Press, Oxford, 1998.

[22] M. R. Bockstaller R. A. Mickiewicz, E. L. Thomas, *Adv. Mater.* **2005**, *17*, 1331.

[23] A. Haryono, W. H. Binder, *Small* **2006**, *2*, 600.

[24] C. De Rosa, F. Auriemma, R. Di Girolamo, G. P. Pepe, T. Napolitano, R. Scaldaferri, *Adv. Mater.* **2010**, *22*, 5414.

[25] A. Malafronte, A. Emendato, F. Auriemma, C. Sasso, M. Laus, I. Murataj, F. F. Lupi, C. De Rosa, *Polymer* **2020**, *210*, 122983.

[26] M. A. Hillmyer, . Adv. Polym. Sci. **2005**, *190*, 137.

[27] F. Auriemma, C. De Rosa, A. Malafronte, R. Di Girolamo, C. Santillo, Y. Gerelli, G. Fragneto, R. Barker, V. Pavone, O. Maglio, A. Lombardi, *ACS Appl. Mater. Interfaces* **2017**, *9*, 29318.

[28] A. Malafronte, F. Auriemma, C. Santillo, R. Di Girolamo, R. Barker, Y. Gerelli, C. De Rosa, *Adv. Mater. Interfaces* **2019**, 1901580.

[29] G. Gaucher, M.-H. Dufresnea, V. P. Sant, N. Kang, D. Maysinger, J.-C. Leroux, *J. Control. Release* **2005**, *109*, 169.

[30] L. Ruiz-Pérez, G. J. Royston, J. P. A. Fairclough, A. J. Ryan, *Polymer* **2008**, *49*, 4475.

[31] M. A. Hillmyer, P. M. Lipic, D. A. Hajduk, K. Almdal, F. S. Bates, *J. Am. Chem. Soc.* **1997**, *119*, 2749.

[32] S. Yang, Z. Liu, Y. Liu, Y. Jiao, *J. Mater. Sci.* **2015**, *50*, 1544.

[33] Y. Takahashi, H. Tadokoro, *Macromolecules* **1973**, *5*, 672.

[34] J. Rieger, *J. Therm. Anal. Calorim.* **1996**, *46*, 965.

[35] DataSheet of the product P9022A-SEO by Polymer Source Inc., https://www.polymersource.ca/index.php?route=product/category&path=2_2190_17_133_745&product_id=10074&subtract=1&serachproduct=yes&categorystart=A-1.1, accessed: May, **2021**.

[36] W. D. Cook, *Polymer* **1992**, *33*, 2152.

[37] M. G. Neumann, C. C. Schmitt, G- C. Ferreira, I. C. Corrêa, *Dent. Mater.* **2006**, *22*, 576.

The table of contents entry should be 50–60 words long and should be written in the present tense. The text should be different from the abstract text.

C. Author 2, D. E. F. Author 3, A. B. Corresponding Author* ((same order as byline))

Title ((no stars))

ToC figure ((Please choose one size: 55 mm broad × 50 mm high **or** 110 mm broad × 20 mm high. Please do not use any other dimensions))